

Electron Correlation via Frozen Gaussian Dynamics

Peter Elliott¹ and Neepta T. Maitra¹

¹*Department of Physics and Astronomy, Hunter College and the City University of New York, 695 Park Avenue, New York, New York 10065, USA*

We investigate the accuracy and efficiency of the semiclassical Frozen Gaussian method in describing electron dynamics in real time. Model systems of two soft-Coulomb-interacting electrons are used to study correlated dynamics under non-perturbative electric fields, as well as the excitation spectrum. The results show that a recently proposed method that combines exact-exchange with semiclassical correlation to propagate the one-body density-matrix holds promise for electron dynamics in many situations that either wavefunction or density-functional methods have difficulty describing. The results also however point out challenges in such a method that need to be addressed before it can become widely applicable.

I. INTRODUCTION

Accurately capturing the correlated motion of electrons in atoms, molecules, and solids remains an active research area today. In ground-state electronic structure problems, the difficulties of solving many-electron systems are rolled up into the correlation energy, a.k.a. *the stupidity energy* [1]. It has been examined in many different scenarios and various limits, but its complexity still haunts us today. Essentially representing the deviation of the many-electron wavefunction from an antisymmetrized product of single-particle orbitals, correlation plays a significant role in time-dependent problems as well. When atoms and molecules are exposed to either perturbative or non-perturbative external fields, fascinating and subtle electron interaction effects mean one must go beyond the “single active electron” picture, yet to solve the time-dependent Schrödinger equation (TDSE) for more than two electrons in strong fields pushes today’s computational limits [2, 3].

The advent of time-dependent density functional theory (TDDFT) in 1984 [4] opened up the possibility of using single-particle orbitals to describe the dynamics of interacting electrons exactly. In TDDFT a single Slater determinant (SSD) in a non-interacting system (the Kohn-Sham (KS) system) is propagated in time, such that it reproduces the exact time-dependent density of the true interacting system. Clearly the KS determinant is not the true interacting wavefunction, nor is it supposed to be an approximation to it; nevertheless by the rigorous theorems of TDDFT all observables of the true, correlated, electronic system can be in principle extracted from it exactly. In practise, approximations are needed for the exchange-correlation functionals, limiting the accuracy of the method. TDDFT is a method of choice in the linear-response regime where the photo-spectra of atoms, molecules and clusters can be found accurately. The computational effort involved scales relatively well, so the spectrum of large systems such as the green fluorescent protein[5], or even candidates for solar cells [6], have been studied.

Although it has proved successful for a wide variety of time-dependent problems [7, 8], its progress for

real-time dynamics in non-perturbative fields has been slower. Three major obstacles involve the lack of memory in the commonly-used functional approximations, lack of good functional approximations to extract observables not directly related to the density, and the inaccuracy of the usual functional approximations when the true wavefunction evolves far from a SSD [9, 10].

Recently a method that accounts for electron correlation semiclassically has been proposed [10] that will, in principle, remedy the aforementioned problems of TDDFT. The method operates within the context of time-dependent density-matrix functional theory (TDDMFT), where the one-body density matrix is propagated in time. The second-order density-matrix enters into the equation for the one-body density-matrix, so is approximated as a functional of the one-body density-matrix in TDDMFT. However it is still difficult to find approximations in TDDMFT that work well when the true wavefunction evolves from being close to a SSD to being far from one [11–13], i.e. those developed so far cannot dynamically change “occupation numbers”. In the proposed method of Ref. [10], a separate semiclassical propagation is done from which the correlation potential is extracted, and used to drive the actual propagation. The approach naturally contains memory effects carried along by classical trajectories, all one-body observables may be immediately extracted, and occupation numbers do dynamically evolve.

Whether the proposed method is accurate for a given application however depends on how close the semiclassical dynamics is to the true dynamics. In the method, only the correlation component of the dynamics is treated semiclassically, while all other terms (including Hartree and exchange), are treated exactly. However, if the semiclassical dynamics deviates far from the true dynamics, the proposed method is unlikely to be accurate. Therefore it is worth investigating how well a semiclassical description of the *entire* dynamics is for the problems of interest. This is the goal of the present paper. We compute the semiclassical dynamics (within the Frozen Gaussian approximation) of model two-electron systems where the exact dynamics can be numerically exactly computed, so that we can

test the accuracy of the semiclassical dynamics against this. We can also compare with the exact KS system: that is, using the exact exchange-correlation potential (that yields the exact density), but comparing observables such as momentum-densities, computed directly from the KS SSD (instead of using the unknown appropriate observable-functionals as in exact TDDFT). Our examples model the following phenomena: states of double-excitation in spectra, dynamics in a strong oscillating field, and population transfer to excited states via resonant driving, or via an optimal field. The chosen systems are one-dimensional models of a quantum dot and a helium atom.

We show both successes and failures of the semiclassical propagation for these applications. We expect however that the proposed method of Ref. [10] is more accurate than such a semiclassical treatment of the entire problem since there it is only the correlation component that is approximated semiclassically. So the results of our studies are expected to improve once applied in the context of the method of Ref. [10].

Our results also have relevance for semiclassical studies of dynamics in their own right (i.e. outside of density-functional-type methods). Although semiclassical treatments of dynamics have seen much interest for nuclear dynamics (eg. Refs. [14–16]), there have only been a few applications to electron dynamics [17–23] and almost all involved a single electron. Part of the reason is that in atoms there is a significant probability that classical trajectories will autoionize after a few cycles in the atomic well: through the electron interaction, one electron gains energy from the other and ionizes while the other drops below its zero-point energy; a process that is classically allowed but quantum-mechanically forbidden. This is a manifestation of what has been called the “zero-point-energy” problem [23–25], and happens also when there are coupled vibrational modes, for example. These trajectories create a lot of noise in the semiclassical sum, making the convergence very difficult, and so are typically terminated. For example, in Ref. [23], accurate spectra of the He atom in both its collinear Zee and eZe configurations were obtained, by discarding trajectories where one electron reaches a certain threshold distance. Theoretically, a question is whether fundamentally these trajectories should be excluded from the semiclassical sum. That is, if the semiclassics could be done with an infinite number of trajectories, whether these trajectories incorrectly contribute to the semiclassical sum. We find that indeed their contribution to the semiclassical sum decreases as more trajectories are added: in this sense, they are valid classical trajectories, and via phase-interference, the semiclassical dynamics restores the zero-point-energy, eliminating their contribution from the semiclassical sum. In practice, nevertheless, we must deal with a finite number of trajectories, so sensible ways to discard these trajectories must be devised. Our results on the model atoms, as well as those on a model quantum dot, lend support to

the conclusions of Ref. [23] that semiclassical dynamics is useful for electrons, for both spectra and dynamics in non-perturbative fields (in some cases). A draw of semiclassics is the interpretive power it carries and we hope to use it also to interpret mechanisms for processes involving interacting electrons, e.g. the role of correlation in multiphoton ionization and multielectron ionization.

The “flavor” of semiclassics explored in the current work is the Frozen Gaussian (FG) dynamics, originally proposed by Heller [26]. This is not one of the rigorous semiclassical propagators that satisfy the TDSE up to order \hbar ; it is however closely related to the rigorous Heller-Herman-Kluk-Kay (HHKK) propagator [14–16, 29–31], which is based on a coherent-state representation of the semiclassical propagator. In Section II, after a brief review of TDDFT and TDDMFT that explains the motivation behind Ref. [10], we review some background regarding FG dynamics and how it is proposed to be used in the method of Ref. [10] in density-matrix propagation. Section III presents results on one-dimensional model systems of two electrons, using FG for dynamics and spectra. Finally, we make some conclusions in Sec. IV.

II. BACKGROUND

In this section, we briefly review TDDFT, the motivation behind going from TDDFT to a density-matrix approach, why we consider a semiclassical approach to correlation, and semiclassical dynamics.

A. TDDFT and its challenges

TDDFT is an exact reformulation of the non-relativistic time-dependent quantum mechanics of many-body systems [4, 8]. It operates by mapping the true problem of interacting electrons into a fictitious, non-interacting system of fermions, called the Kohn-Sham (KS) system, whose one-body density is, in principle, exactly that of the true system, and from which, in principle, all properties of the true system can be obtained. The many-body effects of the interacting system are modelled by a one-body potential, called the exchange-correlation potential v_{xc} . Similar thus in flavor to ground-state density functional theory, its functionals are nevertheless quite different. For example, v_{xc} functionally depends on the entire history of the density, as well as the initial-state of the true system and the initial state of the KS system, $v_{xc}[n, \Psi_0, \Phi_0](\mathbf{r}, t)$ [32]. This *memory-dependence* is however lacking in most of the applications today: they use an “adiabatic” approximation, which simply feeds the time-evolving density into a ground-state approximation:

$$v_{xc}^{\text{adia}}[n, \Psi_0, \Phi_0](\mathbf{r}t) = v_{xc}^{\text{gs}}[n](\mathbf{r})|_{n(\mathbf{r})=n(\mathbf{r}t)} \cdot \quad (1)$$

With this simple approximation, TDDFT has had great success in calculating spectra and response: computationally it scales similar to methods such as time-dependent Hartree-Fock (TDHF) or configuration-interaction singles, but with accuracy that is usually far greater. Yet, this simple approximation is also behind why in some cases approximate TDDFT fails: e.g. to capture states of double-excitation character a frequency-dependent kernel is required [33–35], but the adiabatic approximation yields a frequency-independent kernel.

The lack of memory in the usual functional approximations is also one of the reasons why the application of TDDFT to real-time dynamics applications has not progressed so fast. Model systems for which exact results are available indicate that memory-dependence can sometimes be a crucial factor in the exchange-correlation potential [36–40]. Another difficulty in real-time dynamics, is the problem of “observable-functionals”: although in principle all properties of interest can be extracted from the KS system, it is not known *how* to extract those that are not directly related to the density. One may write these observables as operators on the exact wavefunction, however substituting the KS wavefunction is usually a poor approximation. For example, for momentum distributions, it was shown[9] for a model system with one electron ionizing that the KS momentum distribution incorrectly develops strong oscillations as the electron moves away. In the case of ion-momentum-recoil upon ionization of a model He atom, the KS momentum-distributions were found to be drastically wrong, displaying a single maximum instead of the characteristic two hump structure, and with a significantly overestimated magnitude[41]. Double-ionization probabilities are another example where a more sophisticated observable functional is needed [42].

A third problem arises when the true wavefunction evolves far from an SSD [10, 38]. An illustration of this is in certain quantum control problems, where a laser pulse is found to take the system to a specified target e.g. populating an excited state. For example, a pulse can be found to move the $1s^2$ ground state of Helium to the $1s2p$ excited state. As TDDFT stays in a SSD, with a single doubly-occupied orbital, for all times, it has great difficulty in describing a state that fundamentally is best described by two SSDs. It should be emphasized here that in principle, TDDFT can describe this situation, however the exchange-correlation potential and observable-functionals are extremely difficult to approximate.

B. Time-Dependent Density Matrix Functional Theory (TDDMFT)

To overcome some of the difficulties of TDDFT, we may attempt to use the one-body reduced density ma-

trix, defined below, as the fundamental variable. This has the advantage of containing more information than the density while retaining similar concepts and system-size scaling as TDDFT. An advantage is that functionals for the momentum distribution and kinetic energy are given exactly in terms of the density matrix. The first-order spin-summed reduced density matrix is defined as:

$$\rho(\mathbf{r}', \mathbf{r}, t) = N \sum_{\sigma_1 \dots \sigma_N} \int d^3r_2 \dots d^3r_N \Psi^*(\mathbf{r}'\sigma_1, \mathbf{r}_2\sigma_2 \dots \mathbf{r}_N\sigma_N, t) \Psi(\mathbf{r}\sigma_1, \mathbf{r}_2\sigma_2 \dots \mathbf{r}_N\sigma_N, t) \quad (2)$$

and can be diagonalized by the so-called natural orbitals, $\xi_j(\mathbf{r}, t)$:

$$\rho(\mathbf{r}', \mathbf{r}; t) = \sum_j \eta_j(t) \xi_j^*(\mathbf{r}', t) \xi_j(\mathbf{r}, t) \quad (3)$$

here $0 \leq \eta_j(t) \leq 2$ is the time-dependent occupation number of the j th natural orbital (NO), and $\sum_j \eta_j(t) = N$. We can now interpret the quantum control example discussed at the end of Sec. II A as an issue with the NO numbers. The NOs of the true system will begin with one NO occupation near 2 and the rest close to zero, and will end with two occupation numbers close to 1. The KS system, beginning in the ground-state SSD, has only a single natural orbital which is doubly occupied and time-evolution in the one-body KS Hamiltonian means that the NO occupation number always remains at 2. By using the density matrix of the true system as basic variable instead, we allow the NO occupations to change and thus it should be better than KS at capturing the correct behavior with simpler functional approximations.

The equation of motion for the density matrix is known as part of the BBKGY hierarchy of equations:

$$i\dot{\rho}(\mathbf{r}', \mathbf{r}; t) = \left(-\frac{\nabla^2}{2} + v_{\text{ext}}(\mathbf{r}; t) + \frac{\nabla'^2}{2} - v_{\text{ext}}(\mathbf{r}'; t) \right) \rho(\mathbf{r}', \mathbf{r}; t) + \int d\mathbf{r}_2 f_{ee}(\mathbf{r}', \mathbf{r}, \mathbf{r}_2) \rho_2(\mathbf{r}', \mathbf{r}_2, \mathbf{r}, \mathbf{r}_2; t) \quad (4)$$

where $f_{ee}(\mathbf{r}'\mathbf{r}, \mathbf{r}_2) = 1/|\mathbf{r} - \mathbf{r}_2| - 1/|\mathbf{r}' - \mathbf{r}_2|$ and ρ_2 is the second-order spin-summed reduced density matrix, conveniently decomposed as

$$\rho_2(\mathbf{r}', \mathbf{r}_2, \mathbf{r}, \mathbf{r}_2; t) = n(\mathbf{r}_2) \rho(\mathbf{r}', \mathbf{r}; t) - \rho(\mathbf{r}', \mathbf{r}_2; t) \rho(\mathbf{r}_2, \mathbf{r}; t) / 2 + \rho_c(\mathbf{r}', \mathbf{r}_2, \mathbf{r}, \mathbf{r}_2; t). \quad (5)$$

for a closed-shell spin-saturated system. Atomic units ($e^2 = \hbar = m_e = 1$) are used throughout this paper. Here the terms play the role of Hartree, exchange, and correlation respectively. Setting $\rho_c = 0$ results in the TDHF equations. One could look to close this expression by expressing ρ_c as a functional of ρ and this is the usual approach in TDDMFT. One naturally seeks an adiabatic approximation in which the time-dependent density-matrix is fed into a ρ_2 -functional bootstrapped

from ground-state density-matrix functional theory [43–46] Unfortunately, neither TDHF nor the adiabatic functionals lead to NO occupation numbers changing in time [11–13]. Thus we must look further afield to try and fix this.

A possible solution to this was proposed in Ref. [10] where ρ_C is given by an auxiliary semiclassical dynamics calculation running parallel to the density-matrix evolution. That is, we time-evolve ρ using Eq. 4 with Eq. 5, where all terms are treated exactly quantum-mechanically *except* the last term ρ_C of Eq. 5. This last term is treated as a driving term in this equation, its value obtained from the parallel semiclassical propagation of the system. At each time, the second-order density-matrix, the density matrix, and the density are calculated in the semiclassical system, which then uses Eq. 5 to extract a semiclassical ρ_C . This term is then inserted in Eq. 4 as a driving term. In Ref. [10], it was argued that such an approach addresses the main obstacles TDDFT and adiabatic TDDMFT approaches for real-time dynamics: memory is naturally carried along by the classical trajectories, initial-state dependence is automatically accounted for, all one-body observables may be obtained without the need for further observable-functionals, and NO occupation numbers are time-evolving. We can expect this method to most improve upon the purely semiclassical calculation when in the high-density limit, as the dominating exchange effects will be treated exactly.

Various candidates for the semiclassical method to use in this scheme are possible, with their numerical efficiency inversely related to their semiclassical rigor and accuracy [10]. Most efficient and least accurate is to use a quasiclassical propagation of the one-body Wigner function [27, 28], while least efficient but most rigorous, solving TDSE exactly to order \hbar , is to use the Heller-Hermann-Kluk-Kay (HHKK) propagator [14–16, 29–31]. The Frozen Gaussian (FG) method [26] may be viewed as an approximation to HHKK, and was argued to be a good candidate for use in a “forward-backward” scheme for ρ_C [10]. We focus in this paper therefore on FG dynamics, and our present goal is to investigate how accurate it alone is for electron dynamics. Although in the scheme of Ref. [10], semiclassics is used only for the correlation component of the dynamics, the scheme is likely to be most accurate when the semiclassical propagation of the whole system is reasonably accurate. The purpose of the studies in Section III is therefore to study how accurate FG dynamics on model systems is.

C. Frozen Gaussian Dynamics

Since the earliest days of quantum mechanics semiclassical methods have been explored, for the purpose of interpreting and understanding quantum mechanics via the more intuitive classical dynamics, and also for the purpose of approximation. These methods con-

struct an approximate quantum propagator utilizing classical trajectory information alone. Although there are a variety of forms (e.g. [14, 15, 26, 31, 47–51, 53]), their essential structure is a sum over classical trajectories: $\sum_{\text{cl. traj.}} C_i(t) e^{iS_i(t)/\hbar}$ where $S_i(t)$ is the classical action along the i th trajectory, and the prefactor $C_i(t)$ captures fluctuations around the classical path. Miller [49] showed the equivalence of different semiclassical representations within stationary-phase evaluation of the transformations. Semiclassical formulae have been derived both from largely intuitive arguments (e.g. Heller’s frozen and thawed gaussians Ref.[26, 52]) as well as from rigorous asymptotic analyses of the quantum propagator (see e.g. Refs.[16, 50, 51, 53]) that satisfy TDSE to order \hbar . The latter are based on taking the semiclassical limit of Feynman’s path integral for exact quantum dynamics. This yields a propagator of van Vleck form [50], that requires solving a boundary value problem to find the classical paths eg. from x' to x in time t ; transforming these to “initial-value” representations where instead a sum over an initial coordinate-momentum phase-space is performed, makes the numerics significantly more feasible, especially for longer times and more degrees of freedom.

Semiclassical dynamics captures quantum effects such as interference, zero-point energy, tunneling (to some extent), while generally scaling favorably with the number of degrees of freedom. As the propagator is constructed from classical trajectories, intuition about the physical mechanisms underlying the dynamics can be gained. Although mostly used for nuclear dynamics in molecules, and condensed phases, there have been a handful of applications to electrons [17–23]. The reasons for the reluctance of applying semiclassics to electrons were recently discussed in Ref. [23]. One is that the classical dynamics of interacting electrons are typically mixed with regular and chaotic regions. This makes the semiclassical sum over trajectories increasingly difficult to converge as time evolves. Another is the classical autoionization problem discussed in the introduction; we return to this in Sec. III C. A third problem is that the classical equations of motion become singular at the nucleus, where the potential diverges Coulombically, requiring the need for regularization methods to be applied. As Ref. [17] showed however, this is apparently only a problem when systems are treated in reduced dimensionality: in three-dimensions, no special techniques are required to deal with the Coulomb potential except for a set of measure zero trajectories which hit the nucleus head-on (and these trajectories can be safely discarded). Ref. [23] showed that all these obstacles can be overcome to make semiclassical calculations of atoms and molecules quite practical.

The FG propagation we are exploring can be expressed mathematically as a simplified version of the HHKK propagator [14–16, 29–31] where the N -particle wavefunction at time t as a function of the $3N$ coordi-

nates we denote $\underline{\mathbf{r}}$ is:

$$\Psi^{\text{FG}}(\underline{\mathbf{r}}, t) = \int \frac{d\mathbf{q}_0 d\mathbf{p}_0}{(2\pi\hbar)^N} \langle \underline{\mathbf{r}} | \mathbf{q}_t \mathbf{p}_t \rangle e^{iS_t/\hbar} \langle \mathbf{q}_0 \mathbf{p}_0 | \Psi_i \rangle \quad (6)$$

where $\{\mathbf{q}_t, \mathbf{p}_t\}$ are classical phase-space trajectories in $6N$ -dimensional phase-space, starting from initial points $\{\mathbf{q}_0, \mathbf{p}_0\}$, and Ψ_i is the initial state. In Eq. 6, $\langle \underline{\mathbf{r}} | \mathbf{q} \mathbf{p} \rangle$ denotes the coherent state:

$$\langle \underline{\mathbf{r}} | \mathbf{q} \mathbf{p} \rangle = \prod_{j=1}^{3N} \left(\frac{\gamma_j}{\pi} \right)^{1/4} e^{-\frac{\gamma_j}{2}(r_j - q_j)^2 + i p_j (r_j - q_j) / \hbar} \quad (7)$$

where γ_j is a chosen width parameter and S_t is the classical action along the trajectory $\{\mathbf{q}_t, \mathbf{p}_t\}$. In HHKK, each trajectory in the integrand is weighted by a complex prefactor based on the monodromy (stability) matrix. The pre-factor is time-consuming to compute, and scales cubically with the number of degrees of freedom, but in the FG approximation, it is set to unity. As a consequence, although HHKK solves TDSE exactly to order \hbar , the FG propagator does not; also, although it can be shown that HHKK results are independent of the choice of width parameter γ_j , FG results are not. For all our calculations we take $\gamma_j = 1$. Neither the HHKK propagation nor FG are unitary; typically we find the norm of the FG wavefunction decreases with time, and so we renormalize at every time-step. (In fact for the typically chaotic dynamics of interacting systems, the HHKK prefactor, and norm, grows with time [23]).

The phase-space integral in Eq. 6 is done by Monte Carlo, with the distribution of initial phase-space points weighted according to the initial distribution, $|\langle \mathbf{q}_0 \mathbf{p}_0 | \Psi_i \rangle|^2$. Although Monte-Carlo methods scale as \sqrt{N} for positive integrands, the oscillatory phase can make the FG propagation very difficult to converge. The scheme of Ref. [10] takes advantage of the ‘‘forward-backward’’ nature of the propagation of the second-order density-matrix (i.e in the second-order density matrix, there is both a $\Psi(t)$ and a $\Psi^*(t)$), which leads to some cancellation of phase for more than two electrons. We also observe that the spatial-symmetry of the initial-state is preserved during the evolution (since the Hamiltonian is for identical particles, exchanging coordinate-momentum pairs of two electrons does not change the action). As we study here two-electron singlet states, the wavefunction is spatially-symmetric under exchange of particles.

III. RESULTS+DISCUSSION

We study the accuracy of FG propagation for several different systems involving two soft-Coulomb-interacting electrons in a spin-singlet in one-dimension. Because the TDSE for two interacting electrons in one-dimension can be mapped onto a TDSE for a single electron in two dimensions, the exact problem is eas-

ily numerically solvable, and we can compare our FG results to exact ones. The exact ones are obtained either using the approximate enforced time-reversal symmetry (aerts) algorithm coded in the octopus code [63], or our own exponential mid-point rule code (both use a fourth order Taylor expansion for the exponential). We also comment on how these compare with results using various common approximations in TDDFT for either the exchange-correlation functional (Sec. III A), or for observable-functionals (Secs. III B and III D).

In the latter case, we compute observables from usual operators acting directly on the exact KS wavefunction: this enables us to isolate errors arising from the observable-functional approximation alone (i.e. as opposed to errors from the approximation used for the exchange-correlation potential). For two electrons in a spin-singlet, given the exact time-dependent density, it is straightforward to obtain the exact KS wavefunction [36, 54–56]. We briefly review how. In one-dimension, the continuity equation reads

$$\frac{\partial n(x, t)}{\partial t} + \frac{\partial j(x, t)}{\partial x} = 0, \quad (8)$$

and since the exact KS system reproduces the exact density at all times,

$$j(x, t) = j_{\text{KS}}(x, t) = 2 \Re \phi_{\text{KS}}^*(x, t) \frac{1}{i} \frac{\partial \phi_{\text{KS}}(x, t)}{\partial x}. \quad (9)$$

The last equality follows from the fact that for two electrons in a spin-singlet, there is just one spatial KS orbital ϕ_{KS} (doubly-occupied). Writing ϕ_{KS} as an amplitude times a phase, we deduce,

$$\phi_{\text{KS}}(x, t) = \sqrt{\frac{n(x, t)}{2}} \exp\left(i \int^x \frac{j(x', t)}{n(x', t)} dx'\right). \quad (10)$$

So, the procedure is as follows: we solve the TDSE exactly numerically, finding the exact two-electron correlated wavefunction. The density and current are then extracted from $n(x, t) = 2|\phi_{\text{KS}}(x, t)|^2$ and Eq. (8), and then inserted into Eqs. (10). Usual approximations for observables in TDDFT evaluate the operator corresponding to the observable directly on the KS state; although this is exact for observables directly related to the density, there are errors for other observables, e.g. the momentum-density, which is what we shall look at in examples III B and III D.

In all cases, we will utilize the exact ground-state wavefunction to construct our initial state for propagation. This is to separate out any errors due to a poor ground-state. For a general case where the initial wavefunction is unknown exactly, an appropriate approximate initial state (e.g. sum of a few KS SSD’s, or from a high-level wavefunction calculation) would be used.

A. Hooke Model: Spectra

We begin with the Hooke model for a one-dimensional two-electron quantum dot defined by the Hamiltonian

$$\hat{H}_0 = \sum_{i=1}^2 \left(-\frac{1}{2} \frac{d^2}{dx_i^2} + \frac{1}{2} x_i^2 \right) + \frac{1}{\sqrt{(x_1 - x_2)^2 + 1}} \quad (11)$$

The Hamiltonian becomes separable when written in relative $r = x_1 - x_2$ and center of mass $R = (x_1 + x_2)/2$ coordinates, and we use the quantum numbers of these systems to label the excitations of the full system. In Table I, we give the frequencies of the lowest 8 singlet excitations of this system, along with labels in R, r . The r label must be even in order to have the correct spatial symmetry for a singlet state, while even/odd values for R determine the parity of the state. We have grouped the levels into multiplets whose members become degenerate if the electron-interaction is turned off. Each of the two states in the second and third multiplets are states of double-excitation character: they are mixtures of a single excitation (where, in a non-interacting reference, only one electron is promoted from its ground-state orbital to an excited one), and a double-excitation, where both the electrons occupy excited orbitals [34, 35]. The three states in the fourth multiplet are mixtures of a single-excitation and two double-excitations.

Such states of double-excitation character are well-recognized to be poorly described with the adiabatic approximation in TDDFT, which is used in almost all calculations [33, 34]: instead of producing a multiplet of states, only one state is obtained in the adiabatic approximation, and it has only single-excitation character. In order to find the correct frequencies, TDDFT requires a frequency-dependent kernel to mix the KS single and double-excitations, as was derived in Ref. [34]. The kernel is an *a posteriori* correction to an adiabatic approximation and although it has been recently tested on a variety of systems [57–60], it is not widely used; almost all codes still rely on the adiabatic approximation that fails to capture these. This is the motivation behind our first exploration of the FG dynamics: is semiclassical correlation able to capture states of mixed single and double-excitation character? The answer, as shall see shortly, is yes, at least approximately.

We compute the FG spectra by Fourier-transforming a time-propagation. It is common to start in a linear *kicked* state defined as

$$\Psi_k(x_1, x_2) = e^{ik(x_1+x_2)} \Psi_0(x_1, x_2) \quad (12)$$

where Ψ_0 is the exact ground-state wavefunction, in order to populate the excited states and then to Fourier transform the time-dependent dipole moment, $d(t)$, to

TABLE I: The singlet excitation frequencies $\omega_n = E_n - E_0$, where the ground-state energy $E_0 = 1.774040$ a.u., for the Hooke model. For each excitation, the energy can be written $E_n = E_R + E_r$, where R, r are labels in the center of mass and relative coordinates respectively.

Label (R,r)	ω_n	ω_n^{FG}
1,0	1.000000	1.0
0,2	1.734522	1.6
2,0	2.000000	2.0
1,2	2.734522	2.6
3,0	3.000000	3.0
0,4	3.648334	3.5
2,2	3.734522	3.6
4,0	4.000000	4.0

find the dipole-spectra:

$$d(\omega) = \int dt e^{i\omega t} d(t) \quad (13)$$

The *kick* is equivalent to applying an impulse electric field, $\delta v_{\text{ext}}(x, t) = k\delta(t)x$, to the system[61–64]. For The spectra found this way consists of peaks at the excitation frequencies, the widths of which becomes smaller the longer you propagate the system. For Hooke’s model, this method needs a slight adjustment. In linear response, the *kick* yields a perturbation that is proportional to R , which only couples the ground state (0,0) to the (1,0) state, as the Hamiltonian is simply a harmonic oscillator in this coordinate; the harmonic potential has the special property that a dipole can only connect two states differing by one quantum number. This can also be seen as a consequence of the Harmonic Potential Theorem[65]. So in the exact system, we only see a single peak in the dipole moment when using a linear kick. In order to see higher excitations, we use quadratic and cubic kicks and plot the quadrupole and third-order moments respectively. For example the quadratic kick, $e^{ik(x^2+y^2)}$, in the linear-response regime will be proportional to both R^2 and r^2 , which, using the symmetry and parity discussion earlier, will couple most strongly to the (2,0) and (0,2) states.

We begin the FG calculation in the quadratically *kicked* state (using the exact ground state) with $k = 0.01$ and use 120000 classical trajectories. These trajectories are propagated using the standard leapfrog verlet algorithm for a total propagation time of $T = 200$ a.u with the dipole moment calculated every 0.1 a.u. The power spectrum (absolute value squared) of the quadrupole moment is shown as the solid line in Fig. 1; we use the power spectrum as it is usually more stable than either the purely real or imaginary part, and we also apply the 3^{rd} order polynomial filter given in Ref. [62] to reduce

noise when computing the Fourier transform. We observe two peaks, representing each of the two states in the second multiplet $((0,2),(2,0))$. The FG therefore does capture states of double-excitation character. The exact values of the $(0,2)$ and $(2,0)$ excitations are indicated on the graph as dashed lines. We see that FG gives the peak at $\omega = 2$ a.u. exactly right and the other is shifted lower to approximately $\omega = 1.58$ a.u.. The peak at 2 a.u. is purely an excitation in the center of mass coordinate, where, as mentioned, the system is purely harmonic. For harmonic systems, most semiclassical methods, including FG, are exact [26, 50], and so it is expected that FG works well for this peak.

We reiterate that TDDFT in its usual adiabatic approximation, only yields *one* peak; Ref. [35], examined this pair of excitations using adiabatic exact exchange within the single-pole approximation and found, as expected, a single peak (of frequency 1.87 a.u.).

A quadratic perturbation yields zero transition probability to states of odd parity, such as in the third multiplet. To access these states, we cubically *kick* the system and find the third-order moment, also plotted in Fig. 1 (dashed line). This is a harder test for FG as we are amplifying any errors far from the center in the decaying part of the wavefunction. Again we see that FG works well, giving three peaks corresponding to the first excitation, and the mixed single- and double-excitations in the third multiplet, with again the center-of-mass excitations given exactly. Looking at Table I, we see that the FG correctly reproduces the property that the pair of peaks in the third multiplet differs from those in the second by a single excitation in the center-of-mass coordinate.

The peaks in the fourth multiplet are most clearly resolved by applying a quartic kick to the system. These three states involve mixtures of a single-excitation with two double-excitations, and FG provides a good approximation.

Our spectra could be made cleaner by running for longer times or using harmonic inversion methods for example. However they are adequate for our current purposes of illustrating that the FG method captures correlated states of mixed single and double-excitation character.

In conclusion, although the original motivation for a semiclassical description of electron correlation was to address challenges TDDFT has for real-time dynamics in non-perturbative fields [10], rather than for spectra, this study shows that semiclassical dynamics may nevertheless also be useful in the linear response regime. In particular, FG dynamics does capture states of double-excitation character, albeit approximately, missing in the usual adiabatic approximation of TDDFT. In comparison to the “dressed TDDFT” that uses a frequency-dependent kernel derived in Ref. [34], the FG results are not as accurate, e.g. for the $((0,2),(2,0))$ multiplet, dressed TDDFT gives 1.712 a.u. and 2.000 a.u. On the other hand, in the dressed TDDFT approach, the proce-

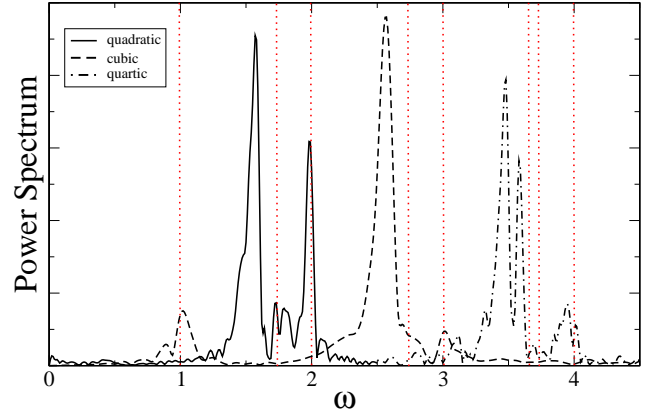


FIG. 1: The power spectra of the Frozen Gaussian quadratic, cubic, and quartic moments for the Hooke’s model dot. The positions of the exact frequencies are shown as the vertical dashed lines.

cedure to obtain the double-excitations involves an identification by the user of zeroth-order single- and double-excitations that are likely to interact strongly, while in the present semiclassical approach, they emerge naturally from the dynamics.

We make two remarks at this point. First, a full HHKK treatment would likely yield more accurate semiclassical spectra, given that the prefactor missing in FG is complex, so its phase contributes interference effects important in determining the resonant frequencies. Second it is important to note that the proposed method of Ref. [10] treats *only* the correlation component of the density-matrix dynamics semiclassically, rather than of the entire dynamics as we have done here; this may result in improved accuracy of the spectra and we shall investigate this in the future. Given the more favorable scaling with system-size of FG than of HHKK, and given that it will ultimately be used in conjunction with exact kinetic, Hartree, and exchange components of the evolution, it is the FG method we are most interested in at present.

B. Hooke Model: Natural Orbitals and Momentum Distributions

Next, we apply a resonant driving perturbation to the Hooke model dot, to investigate whether FG yields time-dependent NO occupation numbers accurately. Due to the harmonic potential theorem [65], applying an electric field does not change the natural orbital occupation numbers; instead we apply a quadratic perturbation, $\delta v_{\text{ext}}(x, t) = k(t)x^2/2$, with a time-dependent spring constant:

$$k(t) = 0.05 \sin(2t) \quad (14)$$

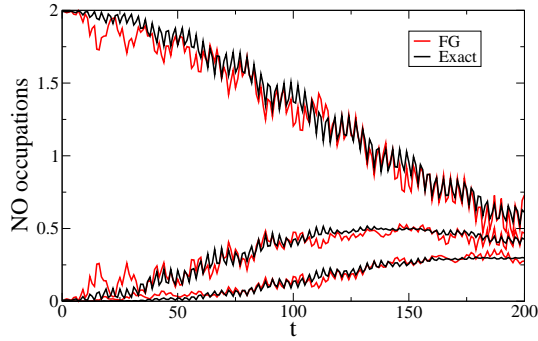


FIG. 2: NO occupation numbers of the Hooke model dot driven at a resonant frequency of 2.0a.u.

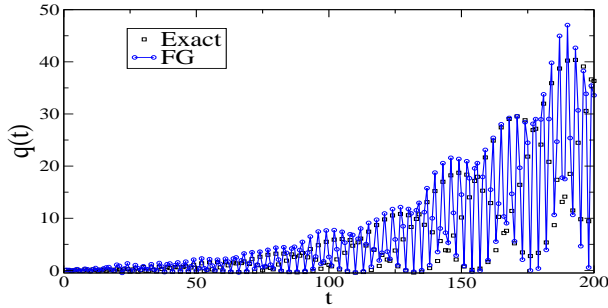


FIG. 3: The quadrupole moment for Hooke model dot driven at resonant frequency. Due to its highly oscillatory behavior, we show the exact values only as square points for clarity.

designed to encourage population transfer to the $(2, 0)$ state.

In Ref. [10], the NO occupation numbers for the Moshinsky model were calculated, however the Moshinsky Hamiltonian is completely quadratic and so, as mentioned, FG is exact. In the Hooke model case, the soft-Coulomb interaction between the electrons makes it a little more realistic model of a quantum dot, and a harder test for FG. In the following FG calculations for the system being driven with Eq. (14), only 60000 classical trajectories were needed for convergence.

In Fig. 2, we plot the exact and FG NO occupation numbers. Recall that for both exact TDDFT and all common approximations in TDDMFT, the occupation numbers are fixed by their initial values and cannot change. It is quite clear that despite not being perfect, FG works very well here, tracking the large changes in the occupation values. The quadrupole moment is shown in Fig. 3, showing that the FG density is also very accurate.

In an exact TDDFT KS calculation, the density would be exact, but the NO occupation numbers would remain at integers 2 (occupied orbital), and 0 for all the rest. We now show how this feature drastically affects observables that are not directly related to the coordinate-space density. We shall focus on the one-body momentum dis-

tribution, defined as

$$n(p; t) = \frac{2}{(2\pi)^2} \int dp' \left| \int dx dx' e^{i(px+p'x')} \Psi(x', x; t) \right|^2, \quad (15)$$

i.e. it is the probability of finding any one electron with momentum p . Although it is known that the momentum distribution of the exact KS wavefunction is not that of the true system [9, 41], little is known about how to extract the latter from the former. In the absence of a good observable-functional for momentum, one resorts to simply using the exact KS momentum distribution.

In Fig. 4, we show the exact, exact KS (computed directly from the exact KS orbital obtained via the procedure in Sec III), and FG momentum distributions at four snapshots in time. The first moment of the KS and exact distributions must integrate to the same value for all one-dimensional systems (in this case zero), due to the facts that $\langle p(t) \rangle = \int dx j(x, t) = \int dx x \dot{n}(x, t)$, and that the KS exactly tracks the density. Despite this, the KS distribution oscillates wildly. The reason for this is not dissimilar to that seen in Ref. [9]: the KS system becomes strongly non-classical as it attempts to describe the system of two-electrons using a single (doubly-occupied) orbital. For short times, the KS $n(p)$ behaves well, however as the breathing motion of the system becomes more pronounced, moving out further and faster, it becomes an increasingly non-classical dynamics for a single orbital, such as in KS, to describe. The underlying phase-space distribution of the KS system develops strong oscillations into negative regions, signifying the non-classical description of different “parts” of one electron moving in different directions. The momentum-distribution represents one observable that the occupation numbers strongly influence. The FG results are much more accurate than the exact KS, as is also reflected in the kinetic energies shown in Fig. 5.

C. Soft-Coulomb Helium: The Problem of Classical Autoionization

Now we move from model quantum dots to model atoms: a soft-Coulomb interaction is used for the nuclear potential, as a one-dimensional model of a Helium atom (see e.g. Refs. [56, 66–69]). The Hamiltonian is given by:

$$\hat{H} = \sum_{i=1}^2 \left(-\frac{1}{2} \frac{d^2}{dx_i^2} - \frac{2}{\sqrt{x_i^2 + 1}} + \epsilon(t)x_i \right) + \frac{1}{\sqrt{(x_1 - x_2)^2 + 1}} \quad (16)$$

where the third term on the first line represents an external electric field applied to the system. This model has been used in several studies of correlated electron dynamics in strong fields as well as in TDDFT, since it

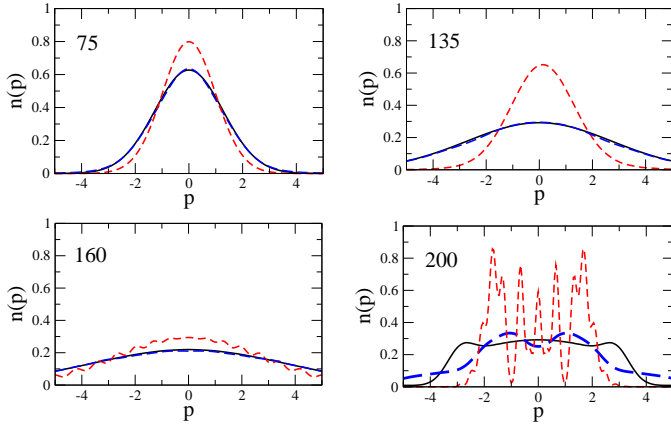


FIG. 4: The exact (solid line), KS (short-dashed line), and FG (long-dashed line) momentum densities calculated at times 75, 135, 160, and 200 au for the on-resonant hooke system.

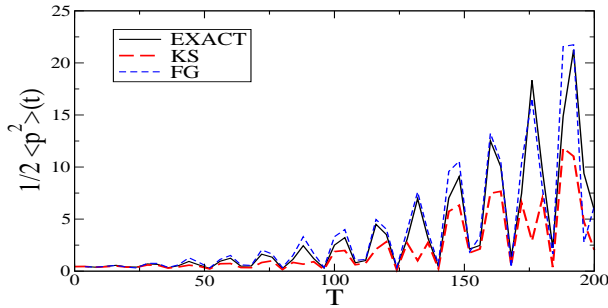


FIG. 5: The kinetic energy for the exact, KS, and FG calculations, when the Hooke dot is driven on resonance. Although the KS system must reproduce the exact momentum, the kinetic energy becomes worse for longer times, while the error in the FG remains about the same.

allows a numerically exact solution to be calculated relatively easily.

With our electronic system no longer everywhere bound, we encounter the problem of classical autoionization, mentioned in the introduction. Even when *no* field is present, this haunts the dynamics, as we will now show. We begin in the exact ground-state of the Hamiltonian Eq. (16) with $\epsilon(t) = 0$. Fig. 6 plots the positions x_1, x_2 of the trajectories in the initial distribution, and where they have evolved to at $T = 10$ a.u. The initial distribution centered at the origin increasingly evolves into a cross, signifying the classical autoionization: one electron zipping off to infinity after stealing the energy from the other left near the origin. Using just 20000 trajectories to compute the FG sum, we plot in Fig. 7 the density at four snapshots in time. Autoionizing wavepackets are clearly seen, evolving out quasiclassically on either side of the central distribu-

tion. (Note that in the exact problem, nothing happens; the distribution remains centered at the origin, as the initial state is an eigenstate.) Although it may appear that the autoionizing packets are growing as a function of time, this is an artifact of the way the FG dynamics is renormalized (see Sec. II C). Before renormalization, the FG norm decreases with time as more trajectories from the central distribution are lost to autoionization and other incoherent effects. Why some of the classically autoionizing trajectories seem to add coherently, forming the wavepackets on the sides, remains to be understood. However choosing a different initial seed to generate the initial distribution results in autoionizing wavepackets centered at different positions moving with different speeds. That is, certainly the results in Fig. 7 are unconverged. In fact, in Fig. 8 we show the effect of increasing the number of trajectories is to significantly decrease the classical autoionization. We deduce that by phase interference in the semiclassical sum, contributions from classically autoionizing trajectories cancel each other out. Considering that HHKK-semiclassics gives the correct dynamics to order \hbar , this is as it should be: Although FG dynamics is not correct to order \hbar a similar effect happens here.

Although these results show that classical autoionization is not a fundamental problem of the semiclassical method, but rather a convergence issue, it does remain an important practical one for most applications; impossibly large numbers of trajectories could be required to make the classical autoionization effect small enough for the purposes. In our following studies we terminate trajectories in one of two ways. In the applications we consider, we do not expect significant amplitude beyond a certain distance. So, (i) we simply terminate any classical trajectory where the coordinate of one electron has reached a prescribed distance, L , away from the nucleus. This is similar to what is done in Ref. [23] in obtaining semiclassical spectra (where the termination distance was additionally dependent on the total energy of the trajectory). Another alternative is to use purely the energy terms to determine autoionization such as was done in Ref. [70]. At all times, this means that we may still observe autoionizing wavepackets peeling off from the central distribution, that eventually reach L , only after which they are discarded; therefore at the earlier times, these may erroneously contribute to the FG. We therefore also consider (ii) prescreening all trajectories, such that if they, at some point during the duration of interest, reach L , they are discarded from the very start of the propagation. (Note this prescreening process is very fast, as only classical dynamics needs to be run; therefore many initial candidate trajectories may be explored). In this way no autoionizing trajectories (as defined by L) ever contribute to the FG sum. In our particular studies, there was some difference between the results obtained with (i) and (ii) especially at shorter times, with (ii) leading to narrower distributions than (i). It is unclear to us which way is more “correct”, especially

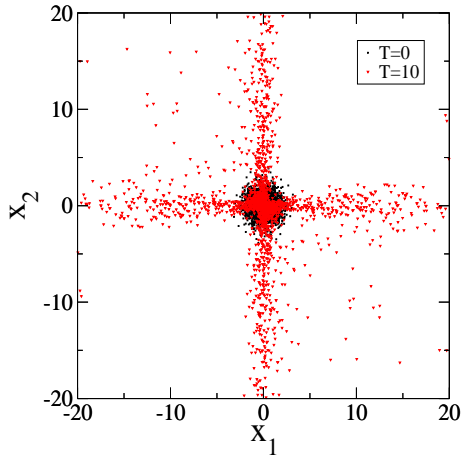


FIG. 6: The positions, x_1 and x_2 , of both particles plotted against each other at the initial time (square points) and at time $t = 10$ a.u. (triangle points). The problem of classical autoionization is characterized by the cross-shape distribution at the later time: one particle falls to the center while the other flies away from the atom.

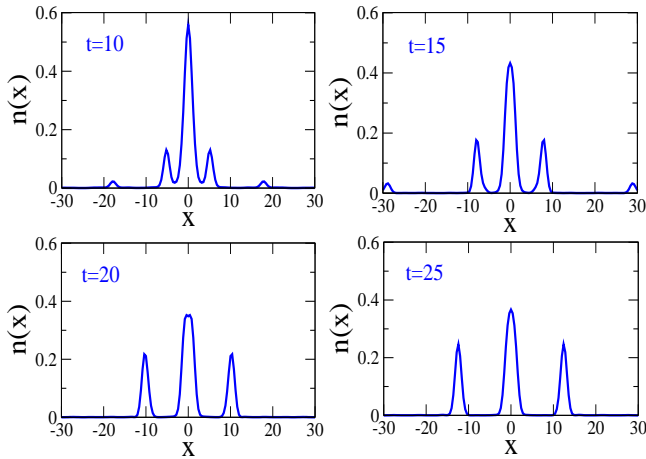


FIG. 7: Snapshots of the FG density at various times when no field is applied to the soft-Coulomb He atom. The lobes on either side of the central distribution represent autoionizing wavepackets. The number of trajectories in the monte carlo sum was $M = 20000$.

given the fact that, theoretically, none of the trajectories are “wrong”: including all, together with their phases, there is no classical autoionization problem. In particular, does the earlier behavior of a trajectory that eventually autoionizes, contribute in a non-cancelling, sensible way to the dynamics at times prior to its autoionizing event? This is an important question we leave for future work.

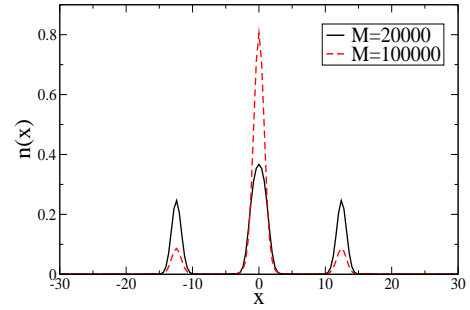


FIG. 8: The FG density at time $t = 25$ a.u. (with no field applied to the soft-Coulomb He atom). Adding more trajectories reduces the classical autoionization.

D. Soft-Coulomb Helium:Strong field

We now apply a relatively strong field to the model He atom:

$$\epsilon(t) = \frac{1}{\sqrt{2}} \cos(0.5t) \begin{cases} \frac{t}{20} & t \leq 20 \\ 1 & t > 20 \end{cases} \quad (17)$$

where the electric field is ramped-up linearly until $t = 20$ au. The value of this field is large enough that classical autoionization effects are relatively small in comparison to the large oscillations in the dynamics induced by the field. We use the procedure (i) described above and terminate trajectories once $|x_i| > 30$ a.u. We found the results were essentially converged starting with 2×10^6 trajectories and finishing with 5×10^5 , the rest being discarded by the termination condition at some point during the run. We plot the NO occupation numbers in Fig. 9, up to a time of 35 a.u. Notice that the number of trajectories needed for convergence in the soft-Coulomb He atom is much larger than those needed in the Hooke-model quantum dot; the latter is almost a best case scenario for semiclassics, because of the quadratic nature of the external potential. The FG captures the change in occupation numbers, perhaps a little too enthusiastically; Figure 10 shows the dipole is also reasonably well approximated. In Fig. 11, we plot the momentum distributions at several snapshots of time, comparing the FG with the exact, and with the exact-KS, as in Sec. III B. We see that the error of the FG remains about the same throughout the evolution, while the error of the KS increases with time. This is a direct consequence of the change in NO occupation numbers: the KS momentum distribution is that of a SSD with NO occupation numbers 2 for one orbital and zero for all others, while that of the true and, roughly captured by FG, changes dramatically in time, as shown in Fig. 9. Consequently, typical observables not directly related to the density, when evaluated using the usual operators on the KS wavefunction become badly approximated; the unknown observable-functionals of exact TDDFT are likely quite complicated.

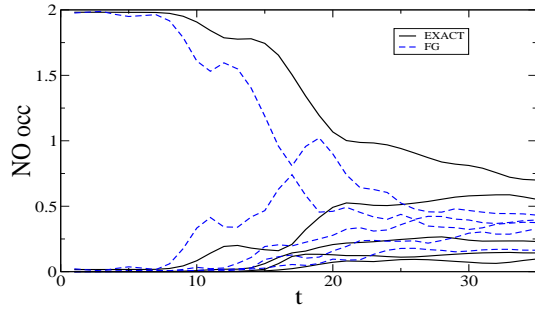


FIG. 9: NO occupation numbers for the soft-Coulomb He atom dynamics induced by Eq. 17.

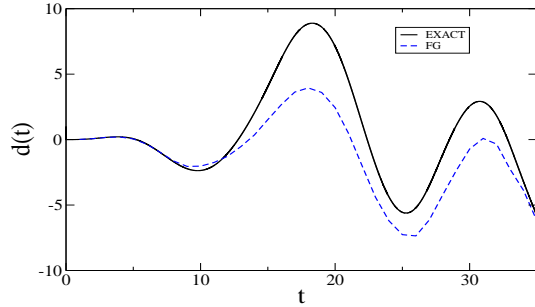


FIG. 10: Comparing the FG dipole moment in the soft-Coulomb He dynamics under Eq. 17.

E. Soft-Coulomb Helium: Towards Optimal Control Theory

Our final example is also the hardest one: we apply an optimal control field to the soft-Coulomb He atom, to try to get it to evolve from the ground-state to the first-excited state. The occupation numbers in the ground-state are close to 2 for the highest, and close to zero for all others, while in the target state, the highest two occupation numbers are both close to 1, having a double Slater determinant character. (See also Sec. II, and [10, 38]). However, instead of optimizing the field for the FG evolution, we simply take an optimal field found for the exact dynamics, and ask how well does it work for the FG problem. (Of course, the former is what we ideally would do, however, we leave the coding of optimal control problems for future work.) We find the optimal field using the optimal control functionality of the octopus code [63, 71]. Moreover, we consider a relatively short duration for the optimal pulse, $T = 35$ a.u., as we will find this illustrates already the challenges the FG approach has for such problems. Because there are only a few cycles of the laser field in this short time, the yield in the exact problem is not very large: the optimal field found in Fig. 12 yields a final state population of 0.73.. The field is significantly weaker than in the previous section, and we really do not expect much ionization, classical or real. To avoid the situation of Fig. 7, we therefore use method (ii) to terminate the trajectories,

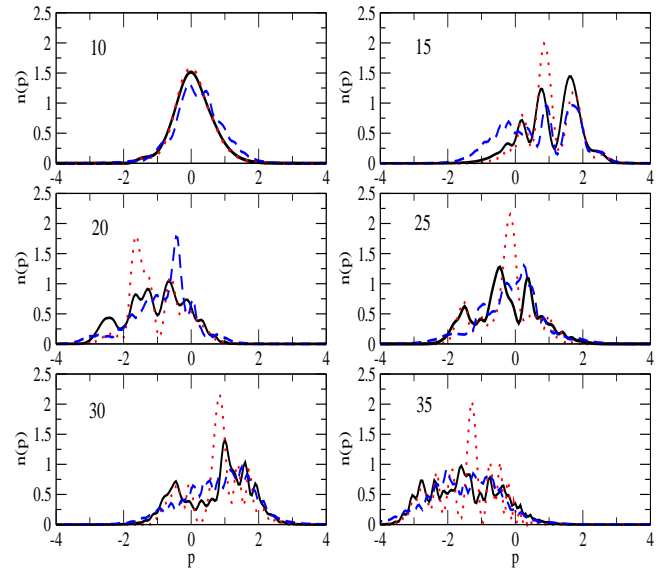


FIG. 11: The momentum density $n(p)$ at times 10, 15, 20, 25, 30 for the strong field case. Solid line is exact, dotted is KS, and short-dashed is FG.

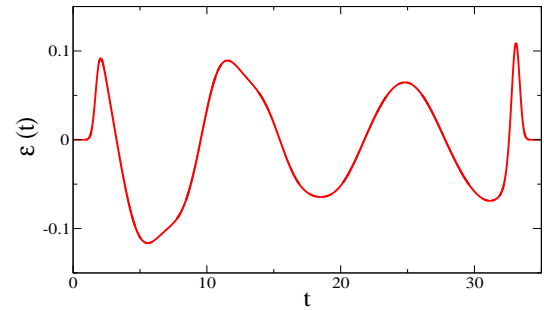


FIG. 12: The optimal electric field to maximally populate the first excited singlet-state of soft-coulomb Helium within a time of 35au.

prescreening them such that no trajectories where one coordinate reaches a distance $L = 10$ a.u. at any time in the run are included. We find that beginning with 5×10^6 candidate trajectories, the prescreening process discards many such that 2391950 remain for the FG calculation.

The result for the NO in in Fig. 13 are disappointing. The FG results are converged, as different seeds, and increasing the number of candidate trajectories did not change the results very much. Also, simply running unscreened calculations with increasing numbers of trajectories, appeared to converge, more or less, to these results. Although initially the largest FG NO occupation number tracks the exact reasonably well, we see that after about $T = 15$, it turns upwards instead of continuing down; the FG state appears to reduce to a SSD instead of developing more of a double -SD character. Turning to Figs. 14 and 15, we see that after beginning to spread, the density then contracts and settles into a narrow distribution in the well. The dipole at shorter times is not

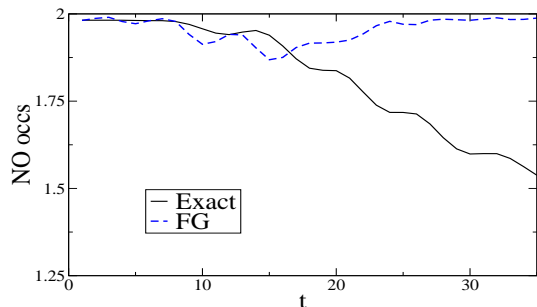


FIG. 13: The highest natural orbital occupation for a pre-screened FG calculation with the optimal electric field of Fig. 12. The exact NO value is nearly 1 at the end, reflecting the double ssd character of the target state.

bad but fails at larger times. We also note that the density appears to tighten as time evolves; this is a consequence of autoionization and occurs even if we do not apply any termination to the trajectories, in the limit of convergence; the predominant trajectories that autoionize are those in the tails of the distribution.

Why the FG results are poor at larger times is, we believe, due to the FG resonant frequencies being so off-set from the true ones, that a field that is optimal for population transfer for one is off-resonant for the other, leading to little transfer. The exact excitation frequency to the first excited state is 0.53, while the FG one is about 0.68 (found by applying a kick to the initial ground-state, as in Sec. III A). For example, in the exact case, if the frequency of the applied field is shifted by as little as 0.05au away from resonance, there is no longer the strong change in NO numbers that we saw in Fig. 2.

Thus the optimal control problem presents an extremely tough test of the frozen gaussian dynamics as it depends critically on subtle interference effects of on-resonance oscillations. As stated in Sec. III A, we expect the FG excitation frequencies to improve when coupled with the TDDM propagation, and hence also improve the optimal control results. This will be investigated in future work.

IV. CONCLUSIONS AND OUTLOOK

The semiclassical FG method provides an intuitive picture of quantum mechanics, as based on classical trajectories, each smeared out into a little fuzzy ball in phase-space, evolving classically in time, and added together with phases determined by their classical action. It, and its more rigorous HHKK version, has also provided useful numerical tools in quantum molecular dynamics. Its application to interacting electronic systems has been hesitant, although recent work [23] clearly shows its promise for electronic spectra. The results of the present work suggest that for systems of interacting electrons in external fields, FG dynamics can

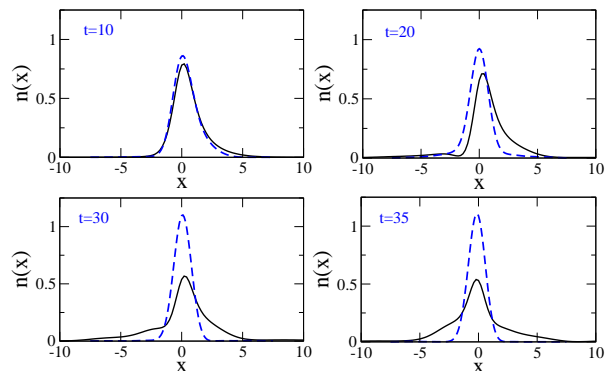


FIG. 14: The density of the pre-screened FG calculation with the optimal field at various times compared to the exact.

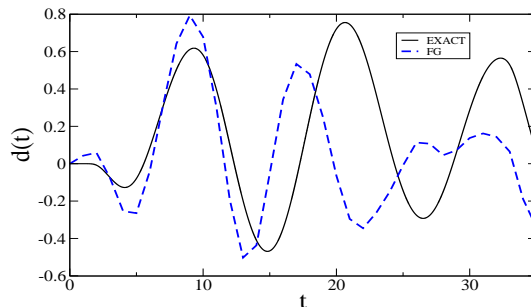


FIG. 15: The pre-screened FG dipole moment versus the exact as a function of time. Although initially the FG mimics the true at short times, the delicate nature of quantum control means FG is too inaccurate for this problem.

also be useful.

In relation to TDDFT and adiabatic TDDMFT, we have shown that FG dynamics overcomes some of the problems these methods have; capturing states of double-excitation character, changing occupation numbers, and accurate momentum distributions. There are nevertheless issues related to its convergence, efficiency and accuracy, that require further study. The issues mainly concern the computational details of the classical trajectories, in particular, the large number of trajectories needed for convergence and also the issue of classical autoionization.

Although a large number of trajectories is required for convergence for our two-electron model atoms, we expect that the “forward-backward” nature of the semiclassical computation in Ref. [10] for the two-body reduced density-matrix will lead to favorable scaling with the number of electrons. Because the prescription of Ref. [10] only calls for the correlation component of the dynamics to be treated semiclassically, less accurate and more efficient semiclassical methods, such as thawed Gaussian or even just quasiclassical propagation (evolv-

ing an initial distribution just classically) may be worth exploring: the aim is just to capture “enough” correlation in a physical way to be used in conjunction with the exact treatment of the one-body terms in the equation of motion for $\rho(\mathbf{r}, \mathbf{r}', t)$.

How to deal with classical autoionization in a consistent and practical way needs further study. When a strong field is present and electrons are unbound at least for some time, the effect of classical autoionization may be relatively small enough for times of interest that a simple termination of trajectories when they get “too far away” makes sense. However in other situations prescreening trajectories by discarding at the start those which at any time reach a given boundary, may be a better approach to avoid autoionizing trajectories “on their way out” from distorting earlier dynamics. Yet there is a delicate balance: if prescreening is done over too long time, too many trajectories that are important at smaller times get discarded. The solution of this problem also depends on what is the quantity of interest, e.g. whether

it is time-resolved densities, or time-averaged spectra.

By including correlation semiclassically, the scheme of Ref. [10] is likely to provide more accurate dynamics than the FG treatment of the entire dynamics shown here, as well as improving over the TDHF and adiabatic TDDMFT results. The present results are encouraging for this next step.

V. ACKNOWLEDGEMENTS

We thank Kenneth Kay and Rick Heller for very helpful discussions. Financial support from the National Science Foundation (CHE-0647913), the Cottrell Scholar Program of Research Corporation and a grant of computer time from the CUNY High Performance Computing Center under NSF Grants CNS-0855217 and CNS-0958379, are gratefully acknowledged.

-
- [1] R. P. Feynman, *Statistical Mechanics*, W. A. Benjamin, New York, 1972.
- [2] J. Parker, L.R. Moore, D. Dundas, and K.T. Taylor, *J. Phys. B: At. Mol. Opt. Phys.* **33**, L691 (2000).
- [3] E. Dehghanian, A. D. Bandrauk, and G. L. Kamta, *Phys. Rev. A* **81**, 061403(R) (2010).
- [4] E. Runge and E.K.U. Gross, *Phys. Rev. Lett.* **52**, 997 (1984).
- [5] M. A. L. Marques, X. Lopez, D. Varsano, A. Castro, and A. Rubio, *Phys. Rev. Lett.* **90**, 258101 (2003).
- [6] N. Spallanzani, C. A. Rozzi, D. Varsano, T. Baruah, M. R. Pederson, F. Manghi, and A. Rubio, *J. Phys. Chem. B* **113**, 5345 (2009).
- [7] P. Elliott, F. Furche, and K. Burke, in *Reviews in Computational Chemistry*, edited by K. B. Lipkowitz and T. R. Cundari (Wiley, Hoboken, NJ, 2009), p. 91.
- [8] *Time-Dependent Density Functional Theory*, eds. M. A. L. Marques, F. Nogueira, A. Rubio, K. Burke, C.A. Ullrich, and E.K.U. Gross (Springer, Berlin, 2006).
- [9] A. K. Rajam, P. Hessler, C. Gaun and N. T. Maitra, *J. Mol. Structure: THEOCHEM* **914**, 30 (2009).
- [10] A.K. Rajam, I. Raczkowska, N.T. Maitra, *Phys. Rev. Lett.* **105**, 113002 (2010).
- [11] K.J.H. Giesbertz, O. V. Gritsenko, and E. J. Baerends, *Phys. Rev. Lett.* **105**, 013002 (2010).
- [12] H. Appel and E. K. U. Gross, *Europhys. Lett.* **92**, 23001 (2010).
- [13] R. Requist and O. Pankratov, *Phys. Rev. A* **83**, 052510 (2011).
- [14] W. H. Miller, *Faraday Disc. Chem. Soc.* **110**, 1 (1998).
- [15] M. Thoss and H. Wang, *Ann. Rev. Phys. Chem.* **55**, 299 (2004).
- [16] K. G. Kay, *Annu. Rev. Phys. Chem.* **56**, 255 (2005).
- [17] G. van de Sand and J.M. Rost, *Phys. Rev. A* **59**, R1723 (1999).
- [18] G. van de Sand and J.M. Rost, *Phys. Rev. Lett.* **83**, 524 (1999).
- [19] K.G. Kay, *Phys. Rev. A* **65**, 032101 (2002).
- [20] T. Van Voorhis and D.R. Reichman, *J. Chem. Phys.* **120**, 579 (2004).
- [21] S. Yoshida, F. Grossmann, E. Persson, and J. Burgdrfer, *Phys. Rev. A* **69**, 043410 (2004).
- [22] S. Takahashi and K. Takatsuka, *J. Chem. Phys.* **124**, 144101 (2006).
- [23] C. Harabati and K. G. Kay, *J. Chem. Phys.* **127**, 084104 (2007).
- [24] W. H. Miller, W. K. Hase, and C. L. Darling, *J. Chem. Phys.* **91**, 2863 (1989).
- [25] J. M. Bowman, B. Gazdy, and Q. Sun, *J. Chem. Phys.* —bf **91**, 2859 (1989).
- [26] E. J. Heller, *J. Chem. Phys.* **75**, 2923 (1981).
- [27] E.J. Heller, *J. Chem. Phys.* **65**, 1289 (1976).
- [28] R. C. Brown and E.J. Heller, *J. Chem. Phys.* **75**, 185 (1981).
- [29] M. F. Herman and E. A. Kluk, *Chem. Phys.* **91**, 27 (1984).
- [30] E. Kluk, M. F. Herman, and H. L. Davis, *J. Chem. Phys.* **84**, 326 (1986).
- [31] F. Grossmann and A. L. Xavier, *Phys. Lett. A* **243**, 243 (1998).
- [32] N. T. Maitra, in Ref.[8].
- [33] D.J. Tozer and N.C. Handy, *Phys. Chem. Chem. Phys.* **2**, 2117 (2000).
- [34] N.T. Maitra, F. Zhang, R.J. Cave and K. Burke, *J. Chem. Phys.* **120**, 5932 (2004).
- [35] P. Elliott, S. Goldson, C. Canahui, and N. T. Maitra, doi:10.1016/j.chemphys.2011.03.020
- [36] P. Hessler, N.T. Maitra, and K. Burke, *J. Chem. Phys.* **117**, 72 (2002).
- [37] N.T. Maitra and K. Burke, *Phys. Rev. A* **63**, 042501 (2001); **64** 039901 (E).
- [38] N.T. Maitra, K. Burke, and C. Woodward, *Phys. Rev. Lett.* **89**, 023002 (2002).
- [39] H. O. Wijewardane and C. A. Ullrich, *Phys. Rev. Lett.* **100**, 056404 (2008).
- [40] C. A. Ullrich *J. Chem. Phys.* **125**, 234108 (2006).
- [41] F. Wilken and D. Bauer, *Phys. Rev. A* **76**, 023409 (2007).
- [42] F. Wilken and D. Bauer, *Phys. Rev. Lett.* **97**, 203001 (2006).
- [43] K. Pernal, O. Gritsenko, and E.J. Baerends, *Phys. Rev. A*

- 75 012506 (2007).
- [44] K. Pernal, K. Giesbertz, O. Gritsenko, and E.J. Baerends, *J. Chem. Phys.* **127** 214101 (2007).
- [45] K. Giesbertz, E.J. Baerends, O. Gritsenko, *Phys. Rev. Lett.* **101**, 033004 (2008).
- [46] R. Requist and O. Pankratov, *Phys. Rev. A* **81**, 042519 (2010).
- [47] E. J. Heller, *J. Chem. Phys.* **94** , 2723 (1991).
- [48] W.H. Miller, *J. Chem. Phys.* **53**, 3578 (1970).
- [49] W. H. Miller, *Adv. Chem. Phys.* **25**, 69 (1974).
- [50] J.H. van Vleck, *Proc. Natl. Acad. Sci. USA* **14**, 178 (1928);
- [51] M. C. Gutzwiller, *J. Math. Phys.* **8**, 1979 (1967).
- [52] E. J. Heller, *Acc. Chem. Res.* **14**, 368 (1981).
- [53] *Techniques and Applications of Path Integration*, L. S. Schulman, (Wiley & Sons, Inc., 1981).
- [54] N. Rohringer, S. Peter, J. Burgdörfer, *Phys. Rev. A* **74**, 042512 (2006).
- [55] M. Thiele, E. K. U. Gross, S. Kümmel, *Phys. Rev. Lett.* **100**, 153004 (2008).
- [56] M. Lein and S. Kümmel, *Phys. Rev. Lett.* **94**, 143003 (2005).
- [57] R.J. Cave, F. Zhang, N.T. Maitra, and K. Burke, *Chem. Phys. Lett.* **389**, 39 (2004).
- [58] G. Mazur, and R. Włodarczyk, *J. Comput. Chem.*, **30**, 811 (2009)
- [59] Mazur, G., M. Marcin, R. Włodarczyk, and Y. Aoki, *Int. J. Quant. Chem.* **111**, 810 (2011).
- [60] M. Huix-Rotllant, A. Ipatov, A. Rubio, and M. E. Casida, *Chem. Phys.* in press (2011).
- [61] K. Yabana and G. F. Bertsch, *Phys. Rev. B* **54**, 4484 (1996).
- [62] K. Yabana, T. Nakatsukasa, J.-I. Iwata, and G. F. Bertsch, *Phys. Stat. Sol. (b)* **243**, 1121 (2006).
- [63] <http://www.tddft.org/programs/octopus/>; M.A.L. Marques, A. Castro, G. F. Bertsch, A. Rubio, *Comput. Phys. Commun.* **151**, 60 (2003).
- [64] M. Thiele and S. Kümmel, *Phys. Chem. Chem. Phys.* **11**, 4631 (2009).
- [65] J. F. Dobson, *Phys. Rev. Lett.* **73**, 2244 (1994).
- [66] J. Javanainen, J. Eberly, Q. Su, *Phys. Rev. A* **38**, 3430 (1988).
- [67] D. Lappas and R. van Leeuwen, *J. Phys. B: At. Mol. Opt. Phys.* **31**, L249 (1998).
- [68] A. Bandrauk, H. Ngyuen, *Phys. Rev. A* **66**, 031401(R) (2002).
- [69] M. Lein, E. K. U. Gross, and V. Engel, *Phys. Rev. Lett.* **85**, 4707 (2002).
- [70] K. Richter, G. Tanner, and D. Wintgen, *Phys. Rev. A* **48**, 4182 (1993).
- [71] A. Castro, J. Werschnik, E. K. U. Gross, submitted; also arXiv:1009.2241v1 (2010).